

## Verification of Ship Resistance under Calm Water Conditions through Numerical Method

Samuel<sup>1,\*</sup>, Muhamad Fadil Audianzah<sup>1</sup>, Eko Sasmito Hadi<sup>1</sup>, Muhammad Luqman Hakim<sup>1</sup>, Muhammad Iqbal<sup>1,2</sup>, Zhang Yongxing<sup>3</sup>

<sup>1</sup> Department of Naval Architecture, Faculty of Engineering, Diponegoro University, Jl. Prof. Soedarto, S.H, Tembalang, Semarang 50275, Indonesia

<sup>2</sup> Department Of Naval Architecture, Ocean, and Marine Engineer, University of Strathclyde, Glasgow, United Kingdom

<sup>3</sup> Nanjing Tianfu Software, Jiulong Lake International Enterprise Park, Jiangning Development Zone, Nanjing, Jiangsu, China

### ARTICLE INFO

### ABSTRACT

#### Article history:

Received 31 January 2023

Received in revised form 16 February 2023

Accepted 4 April 2023

Available online 22 June 2023

#### Keywords:

Frigate; added resistance; axe-bow; CFD; wave generation

The application of an axe-bow design to a Frigate represents a strategic initiative aimed at minimizing total resistance and enhancing ship operation and performance. While ship resistance prediction often prioritizes calm water conditions, this research seeks to broaden the perspective by predicting ship resistance in calm waters according to ITTC recommendations. Employing RANS equations with the  $k-\epsilon$  turbulence model, the study comprehensively predicts and simulates ship resistance and seakeeping behavior. An improved approach employs the Volume of Fluid (VoF) method to solve free surface dynamics, categorizing water and air as distinct phases within Euler's multi-phase flow concept. The integration of Dynamic Fluid Body Interaction (DFBI) is instrumental in predicting ship motion. Through a systematic investigation involving six speeds, the study demonstrates a vigorous alignment between CFD predictions and empirical data, with an error range of 0.12%-2.96%, affirming the CFD method's efficacy in enhancing ship design and operational efficiency.

## 1. Introduction

The Energy Efficiency Operational Indicator (EEOI) was introduced by the International Maritime Organization (IMO) in 2009 to monitor ship operational performance. EEOI allows for an assessment of the operational energy efficiency of ships, which is expressed in CO<sub>2</sub> emissions per unit of transport work [1]. Reducing fuel consumption through slow steaming, and increasing or maintaining propeller efficiency, are several ways to meet this requirement. This aspect can be related to ship resistance, one of the main parameters used for calculations [2]. In order to fulfil this requirement, it is essential to suppress the drag and propulsion performance of the ship on waves to predict the minimum energy consumption level through experiments or numerical simulations.

\* Corresponding author.

E-mail address: [samuelaritonang@lecturer.undip.ac.id](mailto:samuelaritonang@lecturer.undip.ac.id)

However, research on resistance in calm water conditions is still interesting, even though all ships operate in wave conditions. Understanding the hydrodynamic performance of ships in actual sea conditions is an essential aspect of determining ship performance. The wave condition induces the ship movement significantly, which affects drag. The resistance of ships operating at sea is higher than in calm water. The resulting increase in drag can compromise efficient propulsion and can increase fuel consumption. The difference between these two drags arises from the ship's motion and the wave drift forces in the waves. The addition of resistance can reach 15-30% of the total resistance in still water [3].

Research on the added resistance of ships in wave conditions has been carried out for decades. Although methods based on potential theory have been helpful in the realistic design phase, practical results cannot be obtained under high wave conditions or excessive ship motion [4]. Research on added resistance analysis is carried out using the CFD (Computational Fluid Dynamics) method to overcome this limitation. As discussed by the International Towing Tank Conference (ITTC), advances in numerical modelling methods and increased computational power have made it possible to carry out utterly non-linear ship motion simulations using CFD, considering viscosity's effects. In addition, research by Yang and Kim [5], Lee *et al.*, [6], and van Rij *et al.*, [7] showed that the focused waves generated by the CFD program have the same accuracy as the waves generated experimentally and analytically.

Advances in computing technology allow researchers to perform numerical tests. This method is considered more manageable and more efficient than the experimental test. All kinds of problems in real situations can be simulated and validated with experimental data. The CFD method has several approaches to solving fluid flow problems, such as RANS (Reynolds Average Navier-Stokes), LES (Large Eddy Simulation), and DNS (Direct Numerical Solution). The main disadvantage of LES and DNS is that they require more computation memory [8,9]. Therefore, RANS is a solution that is widely used in the shipping industry. Previous CFD studies on added resistance analysis using the RANS method have been carried out. Chen *et al.*, [10] analyzed the motion and added resistance to the S175 container ship. Tezdogan *et al.*, [11] conducted a fully nonlinear unsteady RANS simulation to predict the added resistance of the full-scale KRISO Container Ship model. Yao *et al.*, [12] analyzed additional exercise and resistance for KVLCC2 in regular waves. These studies show promising results for the use of the RANS method.

This study meticulously evaluates turbulent flow enveloping ship hulls, employing the potential RANS solution. It is underpinned by rigorous model experiments at Istanbul Technical University's Ata Nutku Towing Tank to validate and comprehensively assess total resistance. The study uses the standard two-equation  $k-\epsilon$  turbulence model, navigating three stages: a focused initiation with velocity components, followed by methodical scrutiny of pressure dynamics, culminating in computation of turbulence magnitude via the adept overset grid finite volume discretization method. Basically, the main objective is driven by the overarching aspiration to highlight the versatile capabilities within Star CCM+ CFD codes, designed for ship hull design, meticulous analysis, and reliability. Five grid systems (very coarse, coarse, medium, fine and very fine) were used, and the solution of the medium grid was sufficient to study the general flow trends. This study is a starting point for further experiments on additional resistance in waves.

## 2. Material and Method

### 2.1 Object of Research

This study uses a numerical simulation based on the finite volume method to predict motion and resistance. The object of research is using a navy combatant frigate which is included in the category

of semi-planning hull ships. This frigate is a 1:36 scale model with the model number M367 which has been tested experimentally by Hakan *et al.*, [8]. Figure 1 shows the 2-D geometry of the bare hull model. The lines plan is a precision redesign obtained from Hakan *et al.*, [8] research. Figure 2 is a 3D model created using a Non-Uniform Rational B-spline Surface (NURBS), a mathematical computer graphics model. Modelling is conducted by defining lines and surfaces. Figure 3 shows the construction model of the M367 for experimental testing. In the resistance analysis, the wind's effect is not considered. The Dynamic Fluid Body Interaction (DFBI) module serves to address the dynamic movement of the vessel. This enables the solver to assess how the hull moves in response to fluid forces and moments. It accommodates two degrees of freedom, allowing movement in both heave and pitch directions. Details of the main sizes can be seen in Table 1.

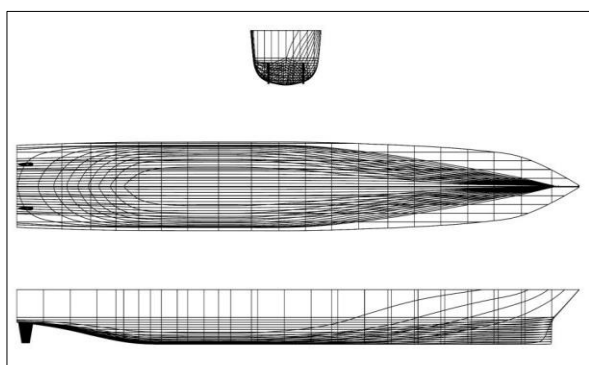


Fig. 1. Lines plan model M367

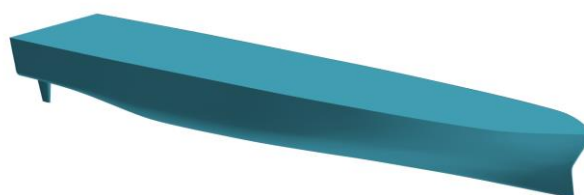


Fig. 2. 3-D views model M 367



Fig. 3. Views of the M367 ship model

Table 1

Main dimension

Main size	Unit	Full scale [8] 1:1	Model scale 1:36
Length of waterline (LWL)	m	139.07	3.866
Length of All (LOA)	m	146.00	4.055
Breadth (B)	m	18.20	0.508
Height (H)	m	11.20	0.31
Draft (T)	m	5.05	0.14
Displacement ( $\Delta$ )	Ton	5768.24	0.124
Block coefficient ( $C_b$ )	-	0.489	0.487
Wetted surface area (WSA)	m <sup>2</sup>	2550.30	1.939

## 2.2 Numerical Approach

The fluid flow equation consists of continuity and Navier–Stokes equations. More complex flows can be handled numerically using CFDs such as the Finite Volume Method (FVM). The RANS (Reynolds-Average Navier-Stroke) equation solves turbulent flow in ship hydrodynamics. The RANS equation has been widely used to solve hydrodynamic problems with incompressible fluids [13]. The Reynolds-Average Navier-Stokes equation, a method of problem-solving based on the principle of conservation of mass and momentum, is used to complete the hydrodynamic simulation. Below is the simplified RANS equation

$$\frac{\partial U_i}{\partial x_i} = 0 \quad (1)$$

$$\frac{\partial U_i}{\partial t} + \frac{\partial(U_i U_j)}{\partial x_j} = -\frac{1}{\rho} \frac{\partial P}{\partial x_i} + \frac{\partial}{\partial x_i} \left( 2\nu S_{ij} - \overline{u'_i u'_j} \right) \quad (2)$$

where  $U_i$  and  $u'_i$  express the mean and fluctuation velocity component in the direction of the Cartesian coordinate  $x_i$ ,  $P$  is the mean pressure,  $\rho$  is the density,  $\nu$  is the molecular kinematic viscosity and  $S_{ij}$  is the mean strain-rate tensor. The strain-rate tensor is defined as

$$S_{ij} = \frac{1}{2} \left( \frac{\partial U_i}{\partial x_j} + \frac{\partial U_j}{\partial x_i} \right) \quad (3)$$

The last term on the right-hand side of Eq. (2) is denoted as the Reynolds stress tensor which is given by

$$\tau_{ij} = -\overline{u'_i u'_j} \quad (4)$$

The Boussinesq (eddy-viscosity) hypothesis obtained with the  $k - \varepsilon$  turbulence model is expressed by

$$\mu_t = -\frac{1}{2} \frac{\rho \tau_{ij}}{S_{ij}} \quad (5)$$

$$\mu_t = c_\mu \rho \frac{k^2}{\varepsilon} \quad (6)$$

The turbulent kinetic energy  $k$  and the rate of dissipation of the turbulent energy  $\varepsilon$  are calculated below

$$\frac{\partial \rho k}{\partial t} + \frac{\partial \rho U_j k}{\partial x_j} = \frac{\partial}{\partial x_j} \left[ \left( \mu + \frac{\mu_t}{\sigma_k} \right) \frac{\partial k}{\partial x_j} \right] + P_k - \rho \varepsilon \quad (7)$$

$$\frac{\partial \rho \varepsilon}{\partial t} + \frac{\partial \rho U_j \varepsilon}{\partial x_j} = \frac{\partial}{\partial x_j} \left[ \left( \mu + \frac{\mu_t}{\sigma_\varepsilon} \right) \frac{\partial \varepsilon}{\partial x_j} \right] + \frac{\varepsilon}{k} (c_{\varepsilon 1} P_k - c_{\varepsilon 2} \rho \varepsilon) \quad (8)$$

When the energy dissipation rate  $\varepsilon$  and the kinetic energy  $k$  are combined, the turbulent viscosity  $\mu_t$  may be determined. A near-wall function uses a realizable  $k$ - $\varepsilon$  two-layer turbulence technique to

describe the velocity profile near the wall Samuel *et al.*, [14], verified hull planning using FVM. The results reveal that CFD can help predict resistance, trim, and point of gravity elevation [14].

### 2.3 Computational Domain and Boundary Condition

Figure 4 is a towing tank dimension that Ozdemir used. In this study, the size of the computational domain is shown in Table 2, and the boundary conditions are shown in Table 3, which refers to the ITTC recommendations [15]. A 2.5 ship length (L) in front of the bow was set as the inlet, and 2.5L behind the transom was designated as the outlet. The bottom was selected as 1.5L under the keel and 1.5L from the deck for the top. The side boundary was set as 2L from the side of the hull, as illustrated in Figure 5. Inlet velocity describes the inlet, bottom, side and top flow limits. A pressure outlet was used for outlet boundaries that are placed far enough to ensure that the fluid flow can develop fully so that flow reflection does not occur. The body surface (Hull) uses no-slip boundary conditions. Taking advantage of the ship's symmetry, only half of the hull and the domains that enter the longitudinal plane were considered in the CFD analysis.

**Table 2**  
Computational Domain

Parameter	Background	Overset
Length (m)	2.5L from FP	0.3 from FP
	2.5L from AP	0.3 from AP
Height (m)	1.5L from deck	1H from deck
	1.5L from keel	1H from keel
Breadth (m)	2L from symmetry	1B from symmetry

**Table 3**  
Boundary conditions

Surface	Boundary conditions
Inlet	Velocity Inlet
Bottom	Velocity Inlet
Side	Velocity Inlet
Top	Velocity Inlet
Outlet	Pressure Outlet
Symmetry	Symmetry Plane
Body	Wall (No Slip)

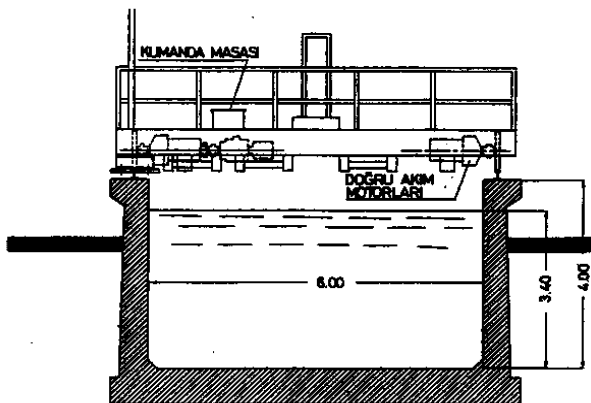


**Fig. 4.** Schematic view of Istanbul Technical University Ata Nutku Towing Tank

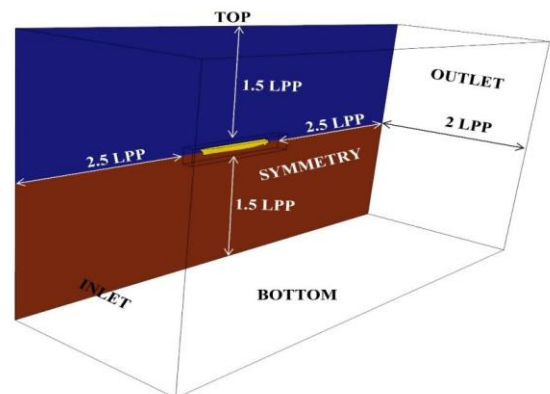


**Fig. 5.** Computational domain and boundary condition

## 2.4 Meshing

Meshing in this study uses the overset mesh method. Overset mesh is a mesh method through donor–acceptor cells. There are two geometries: background as receptor cells and overset as acceptor cells [16]. Research conducted by Yulianti *et al.*, [17] compared overset mesh, morphing mesh and moving mesh methods. As a result, the Overset mesh method showed more accurate results in experimental validation than other methods. But the overset mesh took a long time because the two geometries interact.

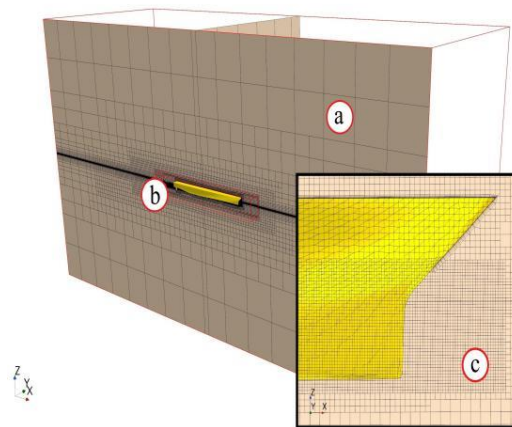


**Fig. 6.** Mesh density at Background (a), Overset (b), and Bow Section (c)

This study used a trimmed-type structured mesh with the anisotropic mesh method to focus on the x, y, and z coordinates. Figure 6 shows the mesh concentration in a particular part, and the mesh density significantly affects the simulation results.

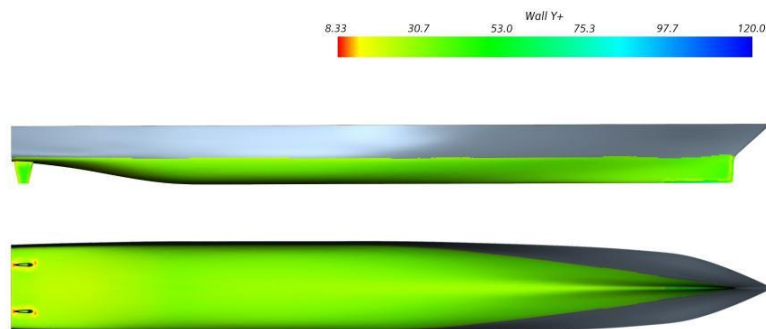


**Fig. 7.** Wall function ( $y^+$ ) on barehull simulation at  $fn = 0.201$

The wall function ( $y^+$ ) was used to bridge the area affected by the viscosity effect between the wall and the turbulent region.  $y^+$  is a non-dimensional unit that is used to capture phenomena at the boundary layer. In previous studies,  $Y^+$  values were used, ranging from 45-110 [8]. Meanwhile, ITTC [15] recommends that  $Y^+$  values be  $30 < y^+ < 100$ . The calculation of  $y^+$  according to ITTC is shown in Eq. (9)

$$Y^+ = \frac{(\rho \cdot U \cdot y)}{\mu} \quad (9)$$

where  $\rho$  is the fluid density,  $U$  is the friction velocity at the wall,  $y$  is the distance from the wall to the first grid node, and  $\mu$  is the dynamic viscosity of the fluid. Figure 7 shows the  $y^+$  values for ships, where the average  $y^+$  values are 50-100. The Volume of Fluid (VOF) method was used to simulate changes in the free surface at the interface between the water and air phases. The time step ( $\Delta t$ ) used in the unsteady simulation must be small enough to complete the movement on the free surface. Time-step is the period interval for each iteration calculation. The time step used for this simulation is a function of the ship's speed ( $V$ ) and the length of the waterline ( $L$ ) recommended by ITTC, which is shown in Eq. (10)

$$\Delta t_{ITTC} = 0.005 \sim 0.01 \frac{L}{V} \tag{10}$$

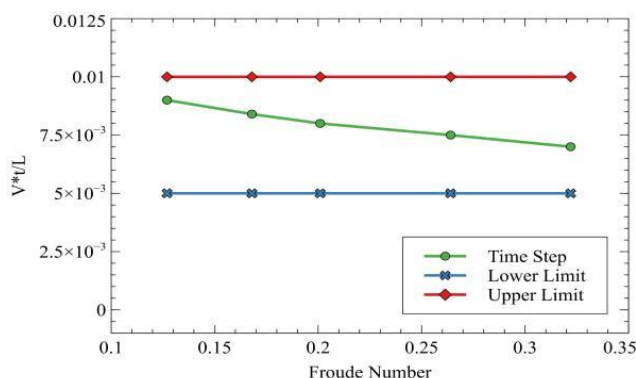


Fig. 8. Time-step scenario

This study's determination of the time step depends on the Courant-Friedrichs-Lewy (CFL) number. The CFL number shows the points the fluid particles pass in that interval. The faster the ship's movement, the smaller the time step used. In this study, the time-step values were taken in the range of 0.0075-0.009, which is visualized in Figure 8. To minimize inaccurate results, apart from comparing with experimental data, it is important to do an independent mesh. It was conducted to ensure that the analysis results stay the same as the mesh density increases [14]. In this simulation, five mesh density conditions were obtained, which are presented in Table 4, and the total mesh is shown in Table 5.

Table 4

Mesh density					
Part name	Very coarse	Coarse	Medium	Fine	Very fine
Bow	0.0020 L	0.0016 L	0.0014 L	0.0013 L	0.0012 L
Stern	0.0020 L	0.0016 L	0.0014 L	0.0013 L	0.0012 L
Free Surface	0.0078 L	0.0065 L	0.0057 L	0.0052 L	0.0049 L
Near Ship	0.0078 L	0.0065 L	0.0057 L	0.0052 L	0.0049 L
Hull	0.0039 L	0.0032 L	0.0025 L	0.0025 L	0.0025 L

Table 5

Total Mesh	
Mesh quality	Total mesh
Very Coarse	779556
Coarse	1227205
Medium	1755342
Fine	2233457
Very Fine	2519969

### 3. Results and Discussion

#### 3.1 Grid Independence Analysis

The mesh size has an essential influence on the computational calculation procedure. The smaller the mesh size, the more accurate the results are, but it takes a long time because of the more significant number of elements. Therefore, an independent mesh is needed to obtain the correct number of elements with stable/dependent results [14].

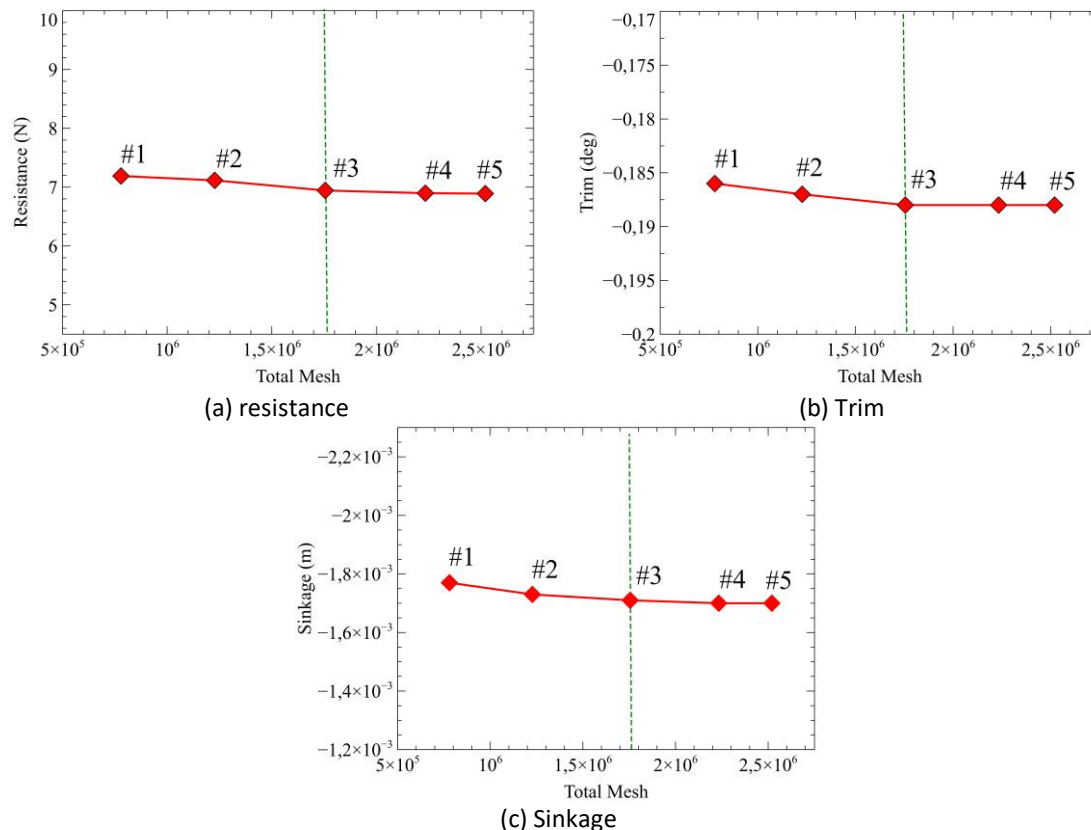
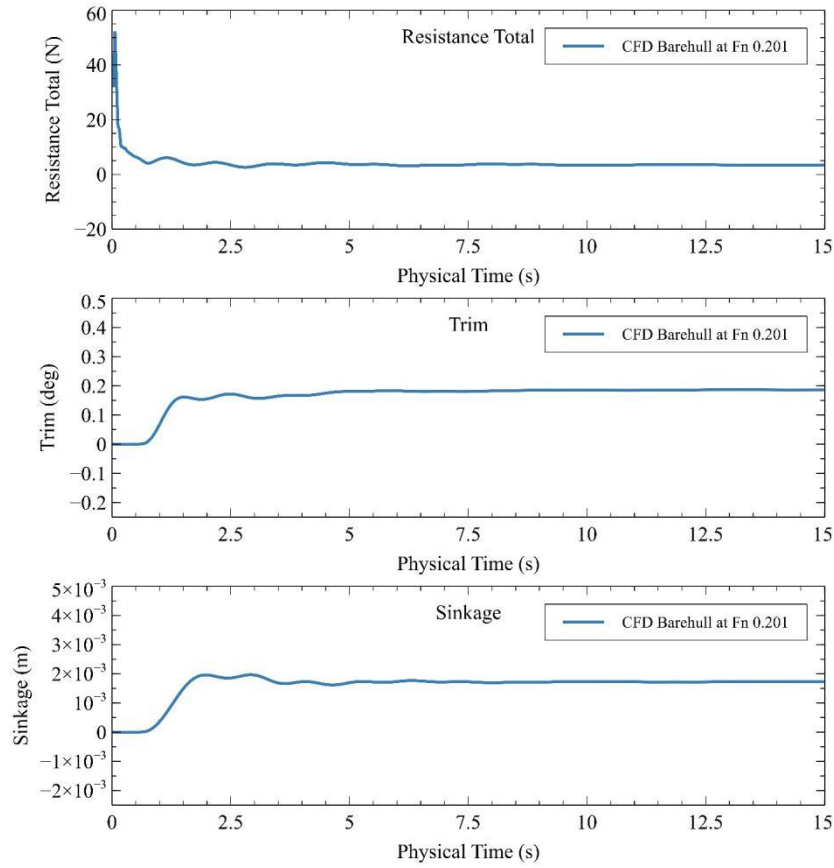


Fig. 9. Mesh independency for resistance (a), trim (b), and sinkage (c) at  $Fn = 0.201$

In Figure 9, Mesh independence was carried out by comparing the simulated values of resistance, pitch, and heave with the number of elements in calm water conditions. Increasing the number of meshes the simulation results become more convergent. The green dotted line shows the convergence limit. Where on grid #3, grid #4, and grid #5, the simulation results show value stability. Compared to grid #4 and grid #5, which require a longer simulation time, the CFD simulation was carried out using grid #3 with a total mesh of 1.75M.

The convergence of model data for resistance, trim, and sinkage values was evaluated over time. In  $Fr 0.201$ , it shows that all data starts to converge when the physical time is 10 seconds. The convergence of data over time is illustrated in Figure 10.



**Fig. 10.** CFD convergence for total resistance, trim and sinkage on bare hull model at  $Fr = 0.201$

### 3.2 Comparison Experiment VS Numerical Results

After determining the number of meshes, validation is carried out by comparing the value of the form factor ( $1+k$ ), the total resistance and the total resistance coefficient from the CFD simulation results with the experimental results. Experiments were carried out at various speeds. ( $1+k$ ) is the form factor, where this value is determined from the resistance test. As the form factor approach ( $1+k$ ) assumes that the viscous resistance is proportional to the coefficient of frictional resistance for a flat plate at the same Reynolds number, the form factor is determined by measuring the total resistance at a low speed. But an accurate measurement of total resistance at very low speeds is questionable. Therefore, the resistance simulation was carried out from  $Fr 0.103$ , considered a low speed, and the results are reasonable [18]. The total resistance coefficient was formulated based on the ITTC shown in Eq. (11), while the form factor calculation can be seen in Eq. (12)

$$C_T = R_T / 0.5 \times \rho \times WSA \times V_s^2 \quad (11)$$

$$1 + k = \lim_{fn \rightarrow 0} \left( \frac{C_T}{C_F} \right) \quad (12)$$

RT is the total resistance,  $\rho$  is the fluid density, WSA is the wetted surface area, and  $V_s$  is the ship's speed. The form factor was calculated using the Prohaska method [19], where the results of the form factor calculation from CFD and experiments are shown in Table 6. The RANS calculation predicted a lower form factor of 1.24% compared to the model test results. A comparison of the total resistance

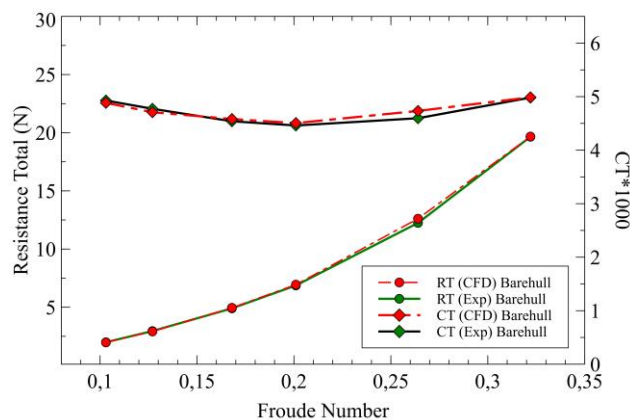
and coefficient between CFD and the experiment can be observed in Table 7. The simulation was carried out at seven different speeds.

**Table 6**  
 The results of form factor

	1+k	Difference
Experiment	1.241	
CFD	1.226	1.24%

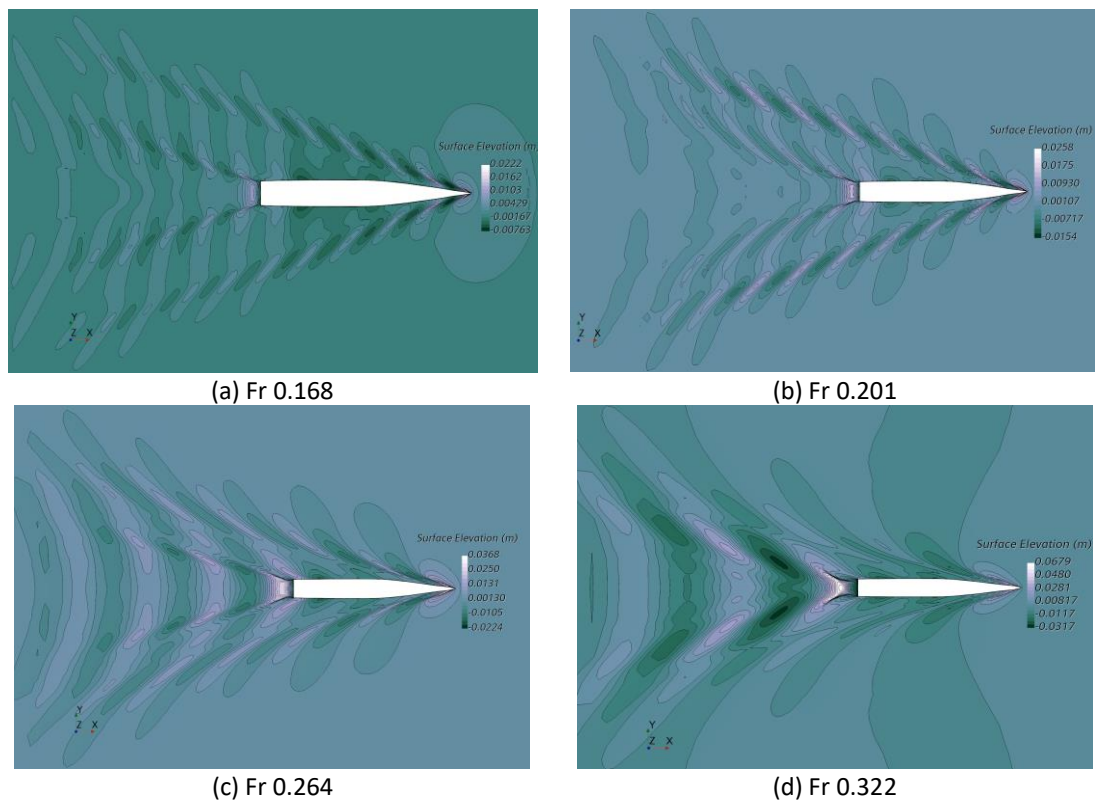
**Table 7**  
 Comparison with experiment

Fr	Vs (m/s)	Experiment [8]		CFD		Error (%)
		R <sub>T</sub> (N)	C <sub>T</sub> x (10 <sup>3</sup> )	R <sub>T</sub> (N)	C <sub>T</sub> x (10 <sup>3</sup> )	
0.103	0.634	1.988	4.928	1.970	4.884	0.89
0.127	0.784	2.947	4.773	2.907	4.709	1.35
0.168	1.037	4.902	4.540	4.947	4.582	0.92
0.201	1.239	6.874	4.461	6.943	4.506	1.01
0.215	1.325	7.845	4.452	7.804	4.541	0.53
0.264	1.628	12.245	4.597	12.608	4.733	2.96
0.322	1.980	19.650	4.982	19.674	4.988	0.12



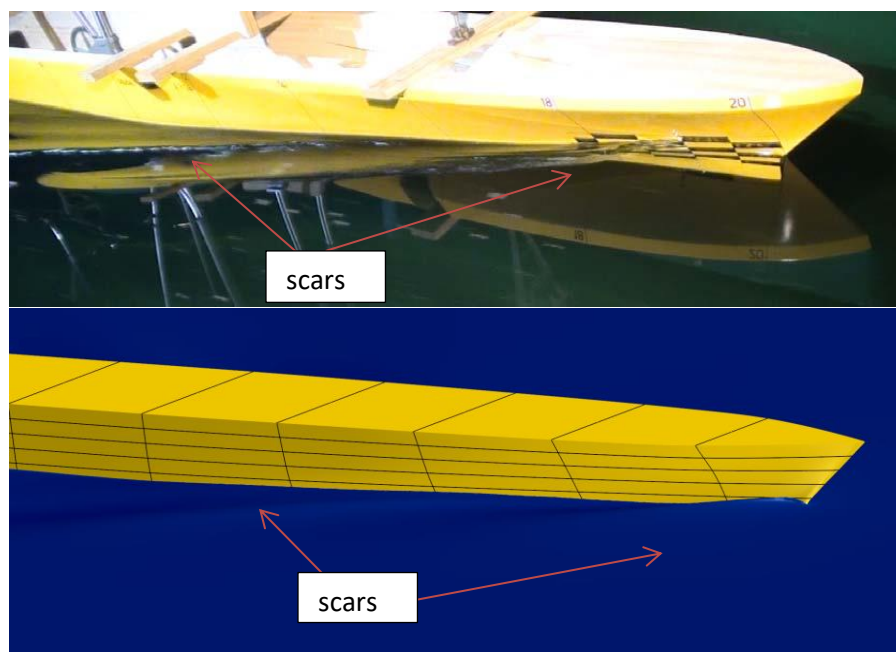
**Fig. 11.** The comparison of total resistance and total resistance coefficient between CFD and Experiment

Figure 11 compares the total resistance and the total resistance coefficient between the CFD model and experimental data in calm water conditions. The CFD simulation shows good results where the total resistances at Fr 0.103 and Fr 0.127 have a smaller value of 0.89% and 1.35% of the experiments. From Fr 0.168 to Fr 0.322, this value is greater than the experiment of 0.12% - 2.96%. Figure 12 shows the calculated wave patterns from the model hull for four different speeds using medium grids, where the bow and stern wave elevations can be clearly seen.



**Fig. 12.** free surface visualization at CFD simulation for 4 different speeds, using medium grids

Figure 13 shows the wave pattern around the bow resulting from CFD simulations and photographs from the experiment result around the ship model at Fr 0.215. CFD simulations show the formation of a thin sheet of water near the bow. Two scars are also visible in the photos during the experiment. Also, according to the data, the CFD simulation shows relatively the same amount of the resulting shoulder waves. Figure 14 shows the development of the simulated waveforms and photos during the experiment behind the model at Fr 0.215. Transom separation can be clearly seen in both CFD simulations and experiments.



**Fig. 13.** Bow wave details for CFD solution (bottom) and experimental photograph (top), Fr 0.215

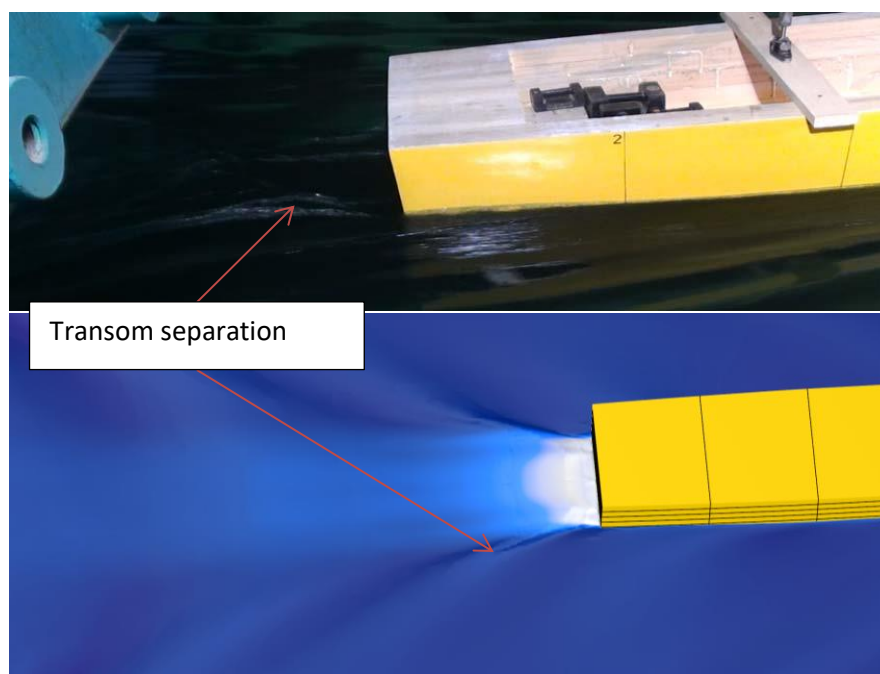


**Fig. 14.** Wake created behind the model, CFD solution (bottom) and experimental photograph (top), Fr 0.215

#### 4. Conclusions

Computational Fluid Dynamics (CFD) is a widely utilized method for solving fluid dynamics equations with high accuracy. This study showcases an impressive correspondence between numerical simulations and experimental data, demonstrating an error range of 0.12% - 2.96%. Leveraging select ITTC recommendations and grid independence studies, CFD proves instrumental in accurately calculating total resistance across various speeds. Notably, congruence between CFD-

generated and empirical wave patterns emerges, underscoring its utility in analyzing the behavior of axe bow ships in regular wave conditions.

### Acknowledgement

This research was not funded by any grant.

### References

- [1] MEPC, IMO. "1/Circ. 684 guidelines for voluntary use of the ship energy efficiency operational indicator (EEOI)." *International Maritime Organization: London, UK* (2009).
- [2] Polakis, Maria, Panos Zachariadis, and Jan Otto de Kat. "The energy efficiency design index (EEDI)." *Sustainable Shipping: A Cross-Disciplinary View* (2019): 93-135.
- [3] Arribas, F. Pérez. "Some methods to obtain the added resistance of a ship advancing in waves." *Ocean Engineering* 34, no. 7 (2007): 946-955.
- [4] Jeong, Kwang-Leol, and Young-Gill Lee. "Numerical simulation of the flow around advancing ships in regular waves using a fixed rectilinear grid system." *Journal of the Society of Naval Architects of Korea* 51, no. 5 (2014): 419-428.
- [5] Yang, Kyung-Kyu, and Yonghwan Kim. "Numerical analysis of added resistance on blunt ships with different bow shapes in short waves." *Journal of Marine Science and Technology* 22 (2017): 245-258.
- [6] Lee, Young-Gill, Cheolho Kim, Jeong-Ho Park, Hyeongjun Kim, Insu Lee, and Bongyong Jin. "Numerical simulations of added resistance in regular head waves on a container ship." *Brodogradnja: Teorija i praksa brodogradnje i pomorske tehnike* 70, no. 2 (2019): 61-86.
- [7] van Rij, Jennifer A., Yi-Hsiang Yu, and Nathan M. Tom. *Validation of simulated wave energy converter responses to focused waves for CCP-WSI blind test series 2*. No. NREL/CP-5000-73861. National Renewable Energy Lab.(NREL), Golden, CO (United States), 2019.
- [8] Hakan Ozdemir, Yavuz, Baris Barlas, Tamer Yilmaz, and Seyfettin Bayraktar. "Numerical and experimental study of turbulent free surface flow for a fast ship model." *Brodogradnja: Teorija i praksa brodogradnje i pomorske tehnike* 65, no. 1 (2014): 39-54.
- [9] Hoa, Nguyen Thi Ngoc, Bich Ngoc Vu, Ngoc Tu Tran, Nguyen Manh Chien, and Tat Hien Le. "Numerical investigating the effect of water depth on ship resistance using RANS CFD method." *Polish Maritime Research* (2019).
- [10] Chen, Si, Takanori Hino, Ning Ma, and Xiechong Gu. "RANS investigation of influence of wave steepness on ship motions and added resistance in regular waves." *Journal of Marine Science and Technology* 23 (2018): 991-1003.
- [11] Tezdogan, Tahsin, Yigit Kemal Demirel, Paula Kellett, Mahdi Khorasanchi, Atilla Incecik, and Osman Turan. "Full-scale unsteady RANS CFD simulations of ship behaviour and performance in head seas due to slow steaming." *Ocean Engineering* 97 (2015): 186-206.
- [12] Yao, Jianxi, Yan Su, Xuemin Song, Zuyuan Liu, Xide Cheng, and Chengsheng Zhan. "RANS Analysis of the Motions and Added Resistance for KVLCC2 in Head Regular Waves." *Applied Ocean Research* 105 (2020): 102398.
- [13] Budiarto, U., S. Samuel, Akbar Adi Wijaya, Serliana Yulianti, Kiryanto Kiryanto, and Muhammad Iqbal. "Stern flap application on planing hulls to improve resistance." *International Journal of Engineering* 35, no. 12 (2022): 2313-2320.
- [14] Samuel, S., Ocud Mursid, Serliana Yulianti, Kiryanto Kiryanto, and Muhammad Iqbal. "Evaluation of interceptor design to reduce drag on planing hull." *Brodogradnja: Teorija i praksa brodogradnje i pomorske tehnike* 73, no. 3 (2022): 93-110.
- [15] ITTC, ITTC. "Recommended procedures and guidelines." *Resistance Test* (2011).
- [16] Kim, D. J., A. Fathuddiin, and A. F. Zakki. "A numerical ventilation problem on fridsma hull form using an overset grid system." In *IOP Conference Series: Materials Science and Engineering*, vol. 1096, no. 1, p. 012041. IOP Publishing, 2021.
- [17] Yulianti, Serliana, S. Samuel, T. S. Nainggolan, and Muhammad Iqbal. "Meshing generation strategy for prediction of ship resistance using CFD approach." In *IOP Conference Series: Earth and Environmental Science*, vol. 1081, no. 1, p. 012027. IOP Publishing, 2022.
- [18] Min, Keh-Sik, and Seon-Hyung Kang. "Study on the form factor and full-scale ship resistance prediction method." *Journal of marine science and technology* 15 (2010): 108-118.
- [19] Prohaska, C. W. "A simple method for evaluation of the form factor and low speed wave resistance." *Proceedings of 11th ITTC* (1966): 65-66.